Supporting information for: Static Disorder in Excitation Energies of the Fenna-Matthews-Olson Protein: Structure-Based Theory Meets Experiment

Marten L. Chaillet,[†] Florian Lengauer,[‡] Julian Adolphs,[¶] Frank Müh,[‡] Alexander S. Fokas,[§] Daniel J. Cole,[‖] Alex W. Chin,[⊥] and Thomas Renger[*,‡]

[†]*Bijvoet Centre for Biomolecular Research, University of Utrecht, Heidelberglaan 8, 3584 CS Utrecht, The Netherlands*

[‡]*Institute of Theoretical Physics, Johannes Kepler University Linz, Altenberger Str. 69, 4040 Linz, Austria*

[¶]*Leibniz Institute for Agricultural Engineering and Bioeconomy, Max-Eyth-Allee 100, 14469 Potsdam, Germany*

[§]*TCM Group, Cavendish Laboratory, 19 J J Thomson Avenue, Cambridge CB3 0HE, United Kingdom*

[‖]*School of Natural and Environmental Sciences, Newcastle University, Newcastle upon Tyne NE1 7RU, United Kingdom*

[⊥]*Centre National de la Recherce Scientifique, Institute des Nanosciences de Paris, Sorbonne Universite, Paris, France*

E-mail: thomas.renger@jku.at

Exciton-vibrational coupling

The fast fluctuation of site energies is described by the exciton-vibrational Hamiltonian

$$H_{\mathrm{ex-vib}} = \sum_m \hbar\omega_\xi g_\xi(m) Q_\xi |m\rangle\langle m| \tag{S1}$$

containing the (dimensionless) coupling constants $g_\xi(m)$ and vibrational coordinate Q_ξ of normal mode ξ of the PPC, the motion of which is described by the vibrational Hamiltonian

$$H_{\mathrm{vib}} = \sum_\xi \frac{\hbar\omega_\xi}{4}\left(Q_\xi^2 + P_\xi^2\right) \tag{S2}$$

containing the vibrational frequencies ω_ξ and the dimensionless coordinate and conjugated momentum Q_ξ and P_ξ, respectively. In principle, also the excitonic couplings could fluctuate, but a normal mode analysis of the spectral density[S1] has revealed that this variation is about two orders of magnitude smaller than that of the site energies. Note that, in general, the exciton-vibrational coupling constants $g_\xi(m)$ and the vibrational frequencies ω_ξ also depend on the conformation c of the PPC. This dependence still needs to be studied and is neglected here for simplicity.

Transformation of the exciton-vibrational Hamiltonian in Eq. S1 to the basis of exciton states $|M\rangle = \sum_m c_m^{(M)}|m\rangle$, defined as the eigenstates of the Hamiltonian H_{ex} (Eq. 1 of the main text) at the equilibrium position of nuclei in the electronic ground state of the complex, gives

$$H_{\mathrm{ex-vib}} = \sum_{M,N} \hbar\omega_\xi g_\xi(M,N) Q_\xi |M\rangle\langle N| \tag{S3}$$

with the exciton-vibrational coupling constant in the exciton basis reading

$$g_\xi(K,M) = \sum_m g_\xi(m) c_m^{(K)} c_m^{(M)}\,. \tag{S4}$$

Due to the partial localization of exciton states, caused by the different site energies of

the pigments, the off-diagonal elements $g_\xi(K,M)$ $(K \neq M)$ are smaller than the diagonal elements $g_\xi(M,M)$[S1]. This inequality is used in the theory of optical spectra below, where the diagonal elements are taken into account exactly and the off-diagonal elements are treated in Markov and secular approximation.

Theory of optical spectra

The optical lineshape function $D_M(\omega)$ of the excitation of the Mth exciton state reads[S2]

$$D_M(\omega) = \frac{1}{2\pi}\int_{-\infty}^{\infty} dt e^{i(\omega-\tilde{\omega}_{M0})t} e^{\gamma_{MM}\{G(t)-G(0)\}} e^{-|t|/\tau_M} \tag{S5}$$

where

$$G(t) = \int_0^\infty d\omega J(\omega)\left\{(1+n(\omega))e^{-i\omega t} + n(\omega)e^{i\omega t}\right\} \tag{S6}$$

contains the spectral density of the site energy fluctuations

$$J(\omega) = \sum_\xi g_\xi^2 \delta(\omega - \omega_\xi) \tag{S7}$$

that is assumed to be the same for all pigments for simplicity, and the Bose-Einstein distribution function of vibrational quanta

$$n(\omega) = \frac{1}{e^{\hbar\omega/k_{\mathrm{B}}T}-1}\,. \tag{S8}$$

The function $G(t)$ contains the diagonal parts of the exciton-vibrational coupling, treated exactly, and gives rise to vibrational sidebands in the lineshape. The frequency

$$\tilde{\omega}_{M0} = \omega_{M0} - \gamma_{MM}E_\lambda/\hbar + \sum_K^{K\neq M} \gamma_{MK}\tilde{C}^{\mathrm{Im}}(\omega_{MK}) \tag{S9}$$

contains the eigenfrequency ω_{M0} of H_{exc} that is renormalized by the diagonal part and the

off-diagonal part of the exciton-vibrational coupling appearing in the second and third terms on the r.h.s., respectively. $E_\lambda = \sum_\xi \hbar\omega_\xi g_\xi^2$ is the reorganization energy of the local electronic transitions and

$$\gamma_{MK} = \sum_m |c_m^{(M)}|^2 |c_m^{(K)}|^2 \tag{S10}$$

contains the coefficients of the exciton wave functions.

For the spectral density $J(\omega)$, we take the functional form extracted from fluorescence line narrowing spectra of the B777-complex[S2] and rescale it such that the Huang-Rhys factor $S = \int d\omega J(\omega)$ equals 0.5, as determined from the temperature dependence of linear absorption spectra of the FMO protein.[S3]

The off-diagonal parts of the exciton-vibrational coupling, treated in Markov and secular approximation, lead to the exciton relaxation-induced lifetime broadening described by the dephasing constant

$$\tau_M^{-1} = \frac{1}{2} \sum_K k_{M\to K} \tag{S11}$$

that contains the Redfield relaxation rate constant

$$k_{M\to K} = 2\gamma_{MK} \tilde{C}^{\mathrm{Re}}(\omega_{MK}) \tag{S12}$$

with

$$\tilde{C}^{\mathrm{Re}}(\omega) = \pi\omega^2 \left\{ (1 + n(\omega)) J(\omega) + n(-\omega) J(-\omega) \right\} . \tag{S13}$$

The $\tilde{C}^{\mathrm{Im}}(\omega)$ in Eq. S9 follows from the above quantity by the principal part integral[S4]

$$\tilde{C}^{\mathrm{Im}}(\omega) = \frac{1}{\pi} \wp \int_{-\infty}^{\infty} d\omega \frac{\tilde{C}^{\mathrm{Re}}(\omega)}{\omega_{MK} - \omega} \tag{S14}$$

The linear dichroism spectrum $LD(\omega)$ is obtained by replacing the $|d_M|^2$ in Eq. 2 of the main text by $|d_M|^2(1 - 3\cos^2\theta_M)$, with the angle θ_M between the exciton transition dipole moment $\mathbf{d}_M$ and the symmetry axis of the FMO trimer. In the calculation of the circular

dichroism spectrum $CD(\omega)$, the $|d_M|^2$ in Eq. 2 of the main text has to be replaced by $\sum_{m,n} c_m^{(M)} c_n^{(M)} \mathbf{R}_{mn} \cdot (\mathbf{d}_m \times \mathbf{d}_n)$ with the distance vector $\mathbf{R}_{mn} = \mathbf{R}_m - \mathbf{R}_n$ and the local transition dipole moments $\mathbf{d}_m$ and $\mathbf{d}_n$ of pigments m and n, respectively.

Finally, we note that the excitonic couplings between pigments in different FMO monomers are so small that they have no influence on the optical spectra. Dynamic localization effects due to the exciton-vibrational coupling restrict the delocalization of exciton states to the monomeric subunits of the FMO protein. Here, we take into account this effect implicitly by restricting exciton delocalization to the FMO monomers.

Static disorder in excitonic couplings

The excitonic couplings for the different conformations of the FMO protein, obtained with FRODA, were calculated with the transition charge from electrostatic potential (TrEsp) method.[S5] Transition charges of non-hydrogen atoms, obtained in earlier work[S5] from a fit of the ESP of the ab initio transition density of the $S_0 \rightarrow S_1$ transition of geometry-optimized BChl *a*, where rescaled to take into account a vacuum dipole strength of 37.1 D^2 determined by Knox and Spring[S6] in an empty cavity analysis of the experimental dipoles strength in different solvents and an average screening/local field correction factor of 0.8 for the Coulomb-coupling between transition densities as determined from Poisson-TrEsp calculations.[S3] The excitonic coupling between pigments m and n follows from these rescaled transition charges as

$$V_{mn}(c) = \sum_{I,J} \frac{q_I(1,0) q_j(1,0)}{|\mathbf{R}_I^{(m)}(c) - \mathbf{R}_J^{(n)}(c)|} \tag{S15}$$

where $\mathbf{R}_I^{(m)}(c)$ and $\mathbf{R}_J^{(n)}(c)$ are the positions of heavy atoms (and corresponding transition charges) of pigments m and n for the conformation c of the FMO protein. Numerical values of the rescaled transition charges are given in Table S3. The distribution functions of the couplings obtained from the different FRODA conformations are Gaussians that are characterized by their FWHM and center positions in Table S4. The optical spectra obtained by

including these coupling fluctuations are compared in Fig. S9 with calculations using constant excitonic couplings. The latter couplings have been obtained from the crystal structure using a point dipole approximation (PDA) and assuming an effective dipole strength of 30 D^2 (as in the TrEsp calculations).[S3] The couplings in PDA are close to the mean values obtained from the FRODA-TrEsp calculations (Table S4) and the inclusion of static disorder in excitonic couplings has practically no influence on the optical spectra (Fig. S9).

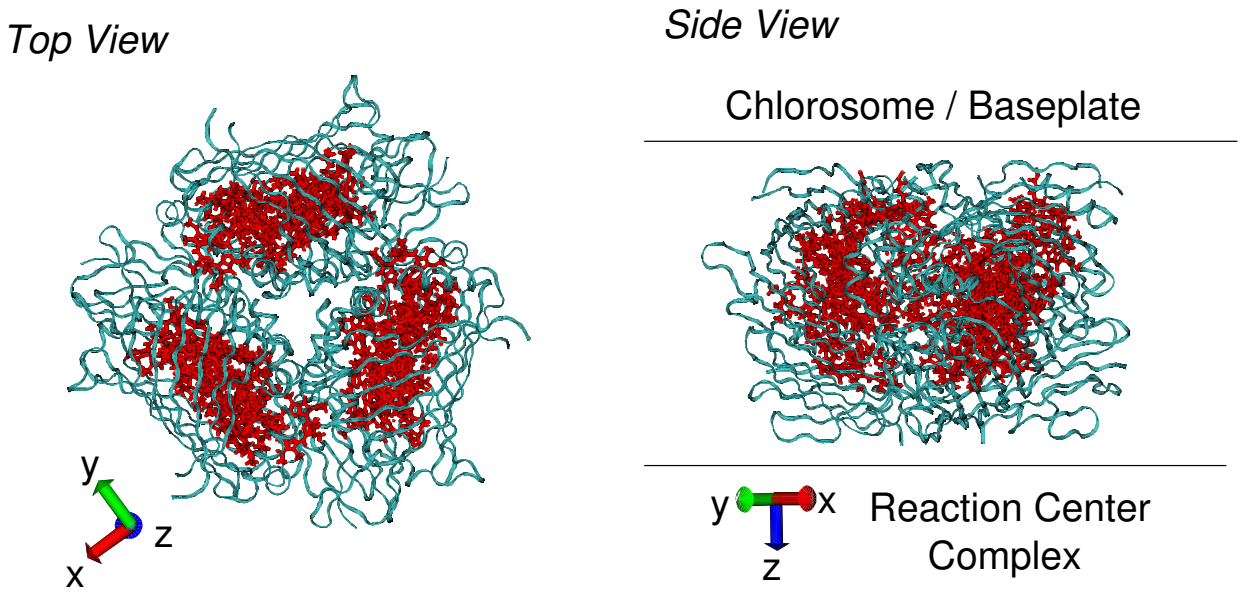

Figure S1: Complete structure of the trimeric FMO protein of *P. aestuarii*[S7] in top view from the direction of the chlorosome towards the reaction center complex (left part) and in a side view (right part). Each monomeric subunit binds 8 BChl *a* pigments, which are shown in red. The protein is shown in ribbon style. An enlarged view of a monomeric subunit is provided in Fig. 1 of the main text.

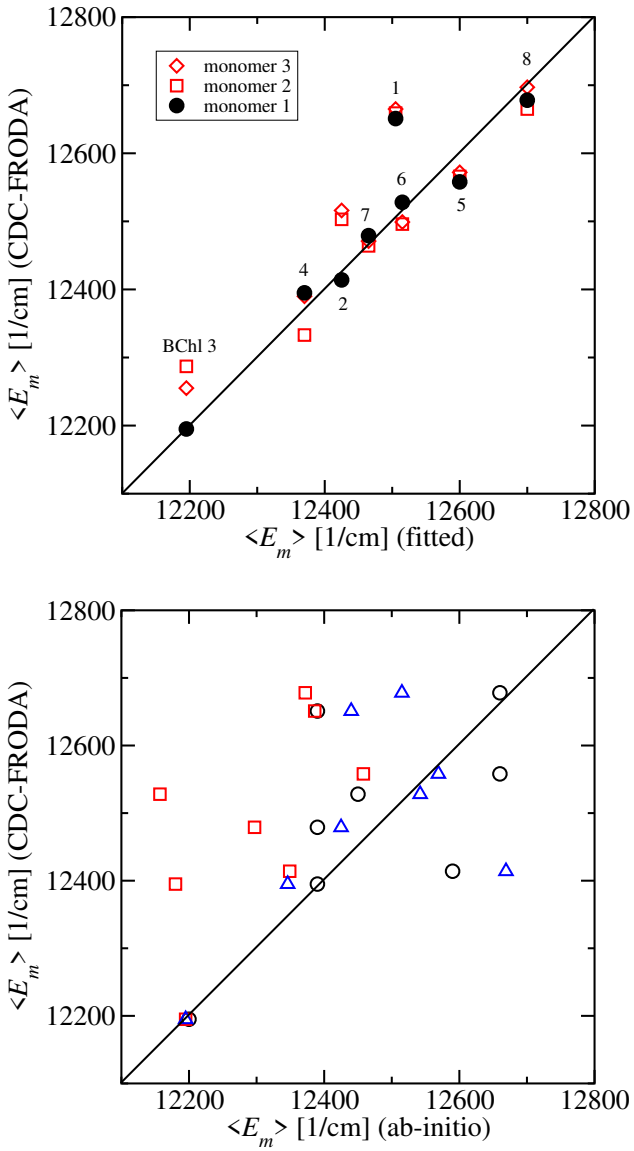

Figure S2: **Upper part**: Correlation between the mean site energies $< E_m >$ (fitted) obtained earlier[S8] by CDC calculations and fits of experimental spectra and the mean site energies $< E_m >$ (CDC − FRODA) obtained here from the FRODA/CDC calculations for the three monomeric subunits of the FMO protein. **Lower part**: Correlation between the $< E_m >$ (CDC − FRODA) site energies of monomer 1 and ab-initio calculations from the literature: QM/MM with Shepard interpolation correction[S9], applying a constant shift of -1720 cm^{-1} to all ab-initio site energies (black circles), QM/MMPol with short-range corrections from Table S4 of the supporting information of ref.[S10], applying a constant shift of -1679 cm^{-1} (red squares), and QM/MM-QM/EFP (Fig. 4 of ref.[S11], applying a constant shift of -2390 cm^{-1} (blue triangles). The latter calculations were performed on *Chlorobaculum tepidum* formerly known as *Chlorobium tepidum*, whereas all other calculations refer to *Prostecochloris aestuarii*. Note, that both species are expected to have similar site energies.[S3] The diagonal lines in the upper and lower graphs illustrate a perfect correlation.

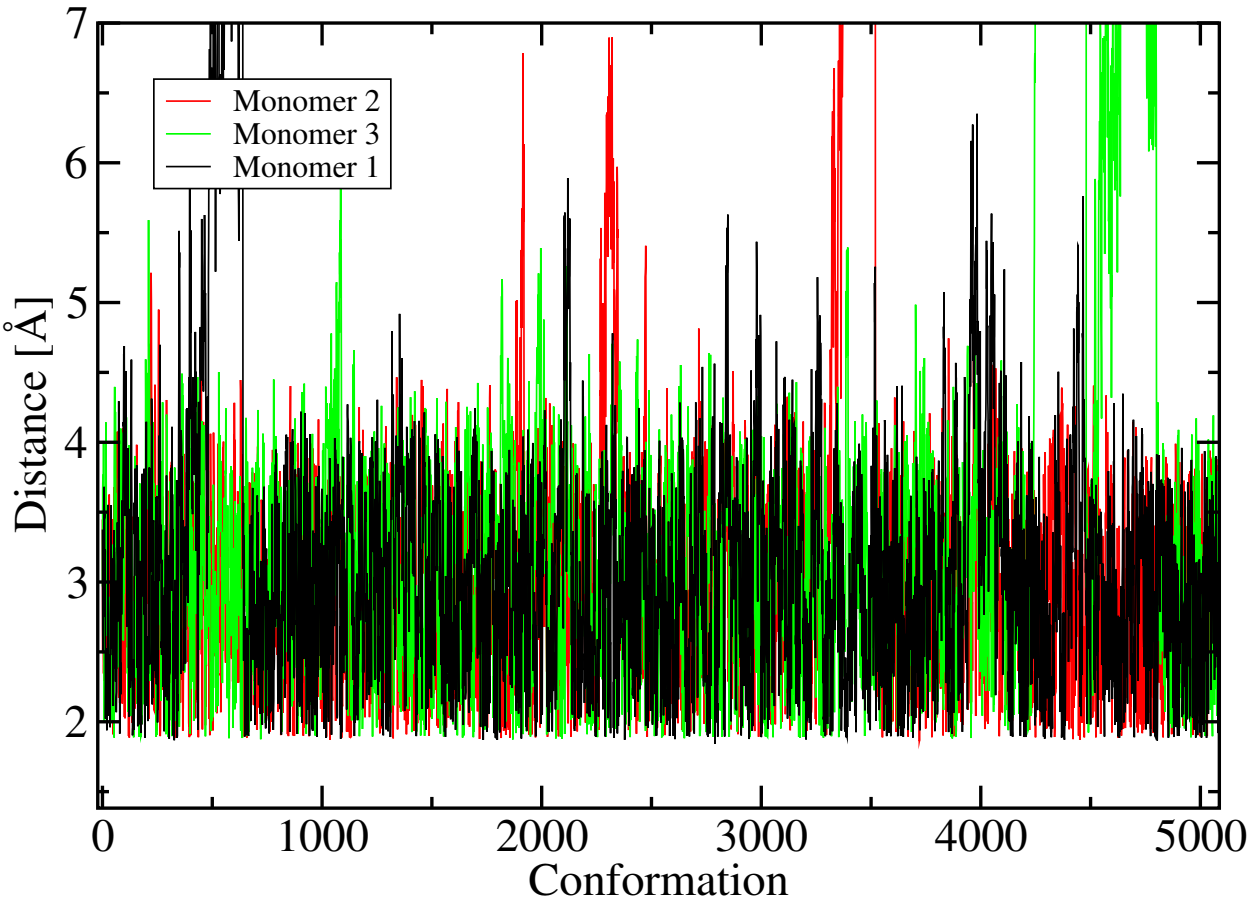

Figure S3: Distance between the oxygen atom of a water molecule in the neighborhood of BChl 1 and the oxygen atom of the 3-acetyl group of BChl 1 in the three monomeric subunits of the FMO protein in the course of the FRODA MC simulations. The large amplitude of the distance variations indicates that the hydrogen bond between the two oxygen atoms is not stable.

Table S1: Centers $< \Delta E_m >$ and FWHM of the Gaussian distribution functions of site energy shifts of the BChls ($m = 1, ..., 8$) in monomer 1 (Fig. 3 of the main text) and in monomers 2 and 3. All quantities in units of cm^{-1}.

	Monomer 1		Monomer 2		Monomer 3	
m	$< \Delta E_m >$	FWHM	$< \Delta E_m >$	FWHM	$< \Delta E_m >$	FWHM
1	90.7	86.9	98.6	84.5	105.1	88.0
2	-145.9	107.0	-56.8	133.9	-44.1	125.3
3	-364.7	128.6	-273.2	167.1	-304.6	159.9
4	-165.4	93.0	-227.0	96.7	-170.1	106.1
5	-2.4	85.9	5.9	86.2	11.8	86.3
6	-32.1	151.4	-63.5	129.2	-61.1	119.6
7	-81.5	118.6	-95.7	108.8	-88.8	114.9
8	117.5	217.6	105.2	220.8	137.4	218.1

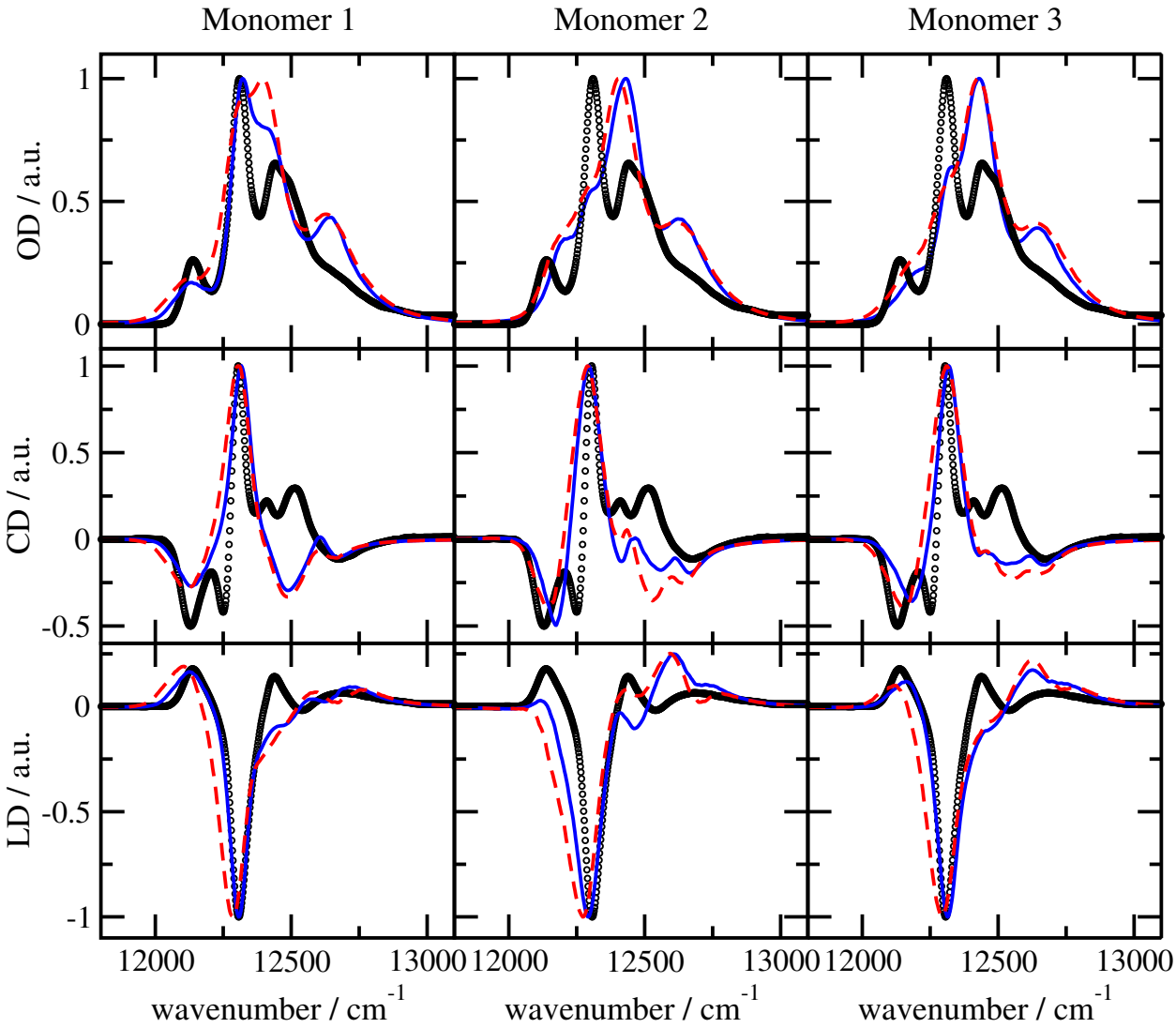

Figure S4: Low-temperature (4 K) optical spectra of the three monomeric subunits of the FMO protein, calculated by neglecting (blue solid lines) or taking into account (red-dashed lines) the interaction of pigments with water molecules, are compared with experimental data[S12] (black circles).

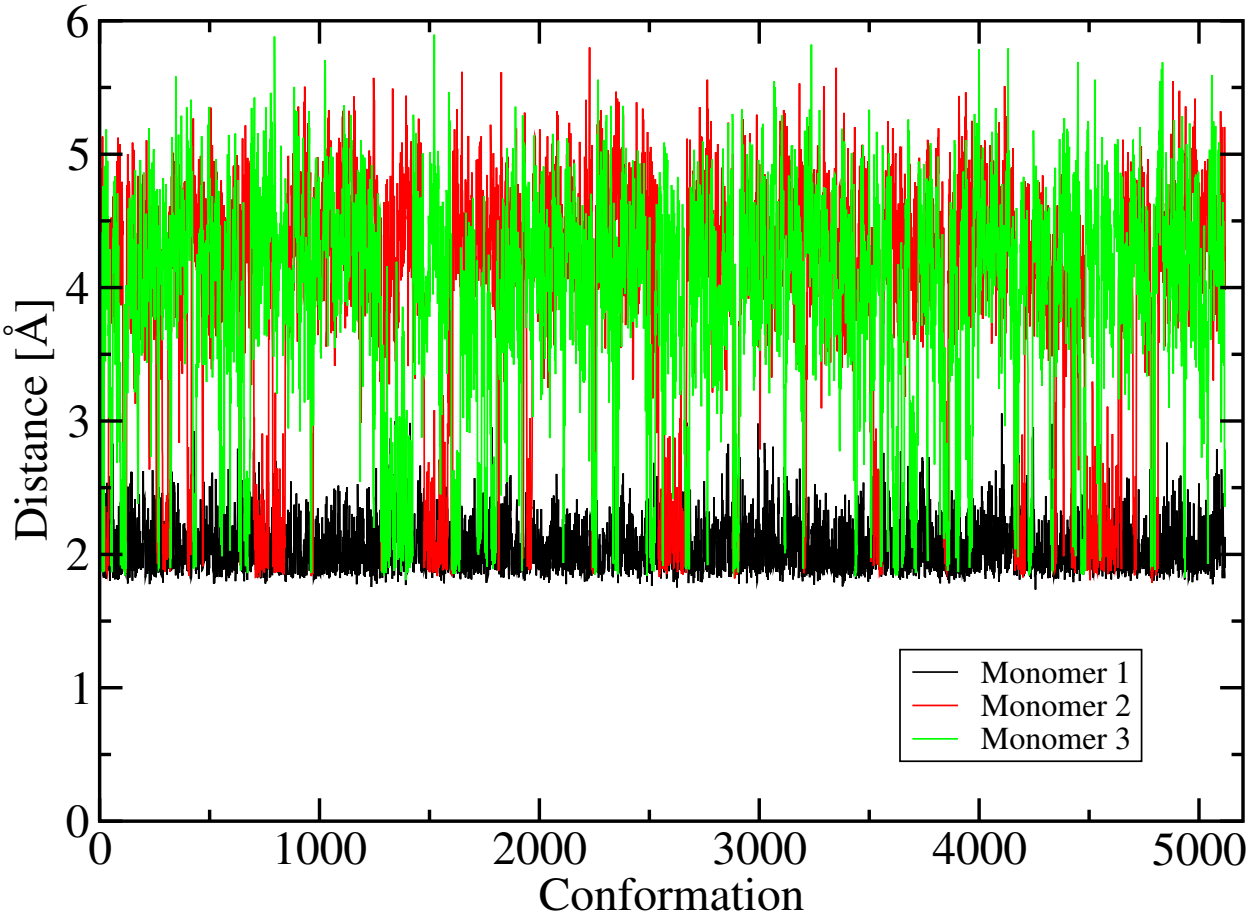

Figure S5: Distance between the hydroxy oxygen atom of Ser 72 and the oxygen atom of the 3-acetyl group of BChl 2 in the three monomeric subunits of the FMO protein in the course of the FRODA MC simulations. The data indicate that in monomer 1, the hydrogen bond is permanently formed, whereas it is broken for most of the conformations in monomers 2 and 3.

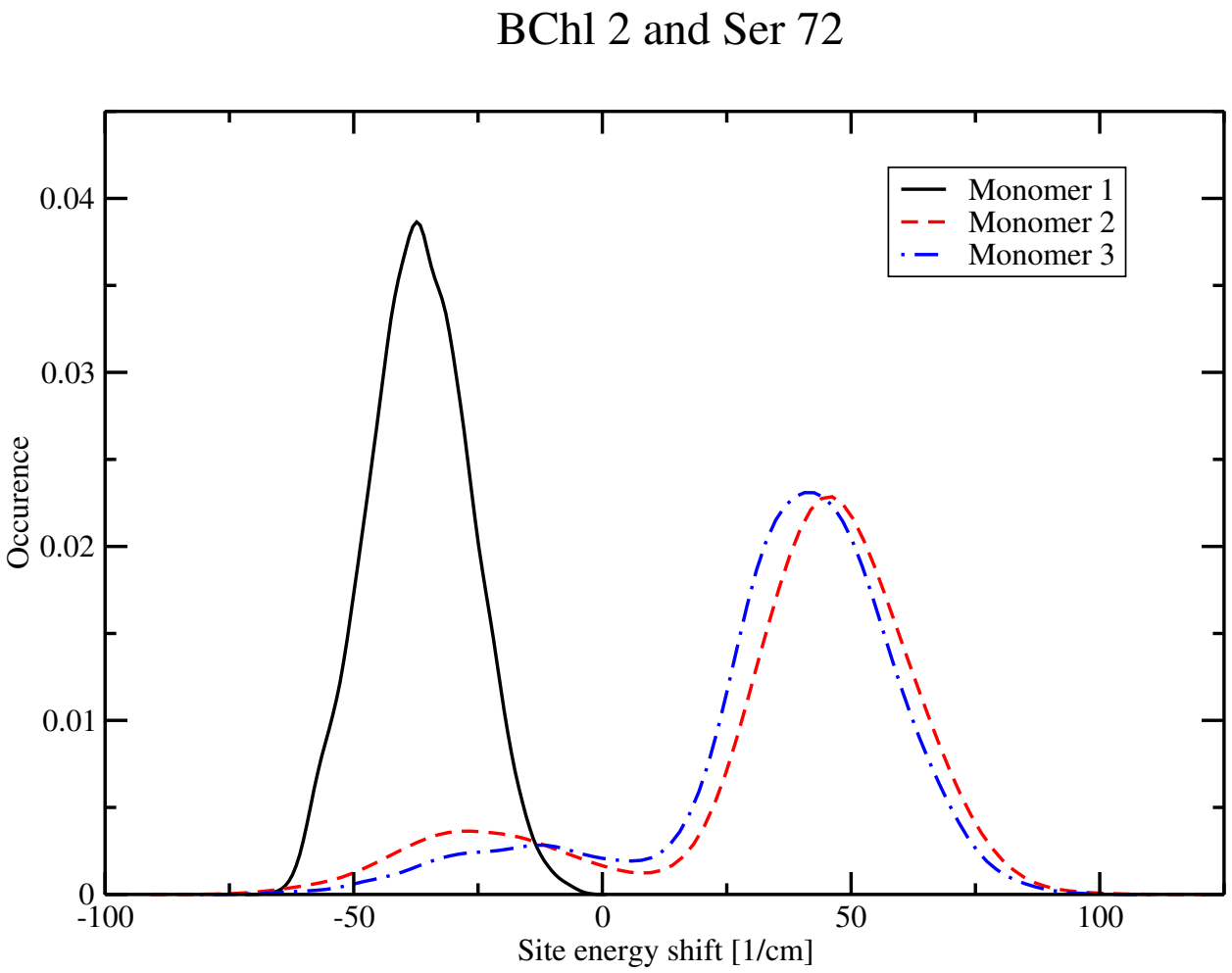

Figure S6: Distribution of site energy shift of BChl 2 caused by Ser 72 in the three monomeric subunits of the FMO protein, obtained from histograms of $\Delta E_2^{(\mathrm{Ser72})}$ (Eq. 4 of the main text).

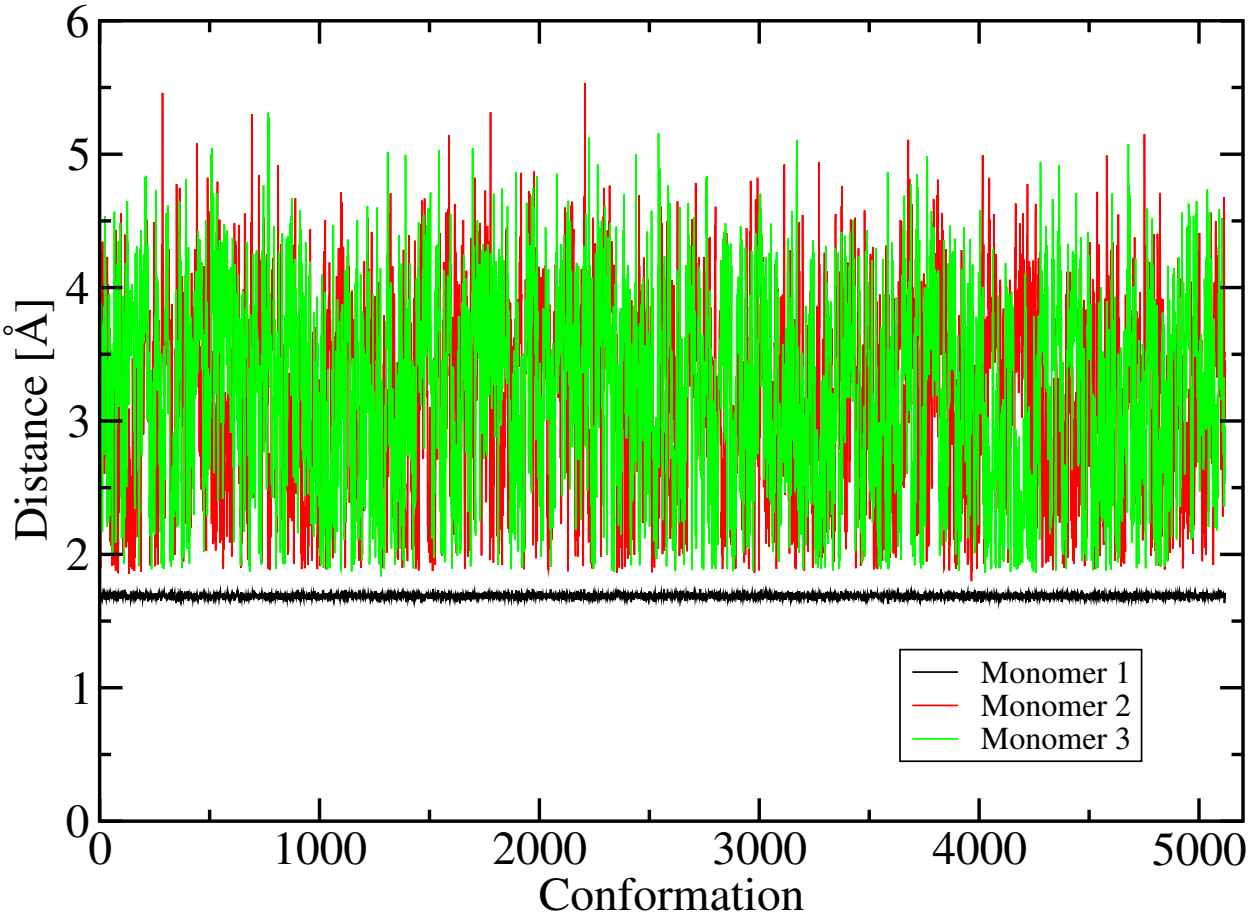

Figure S7: Distance between the hydroxy oxygen atom of Tyr 15 and the oxygen atom of the 3-acetyl group of BChl 3 in the three monomeric subunits of the FMO protein in the course of the FRODA MC simulations. The data indicate that there is a strong, stable hydrogen bond in monomer 1, whereas the hydrogen bond is broken in most of the conformations in monomers 2 and 3.

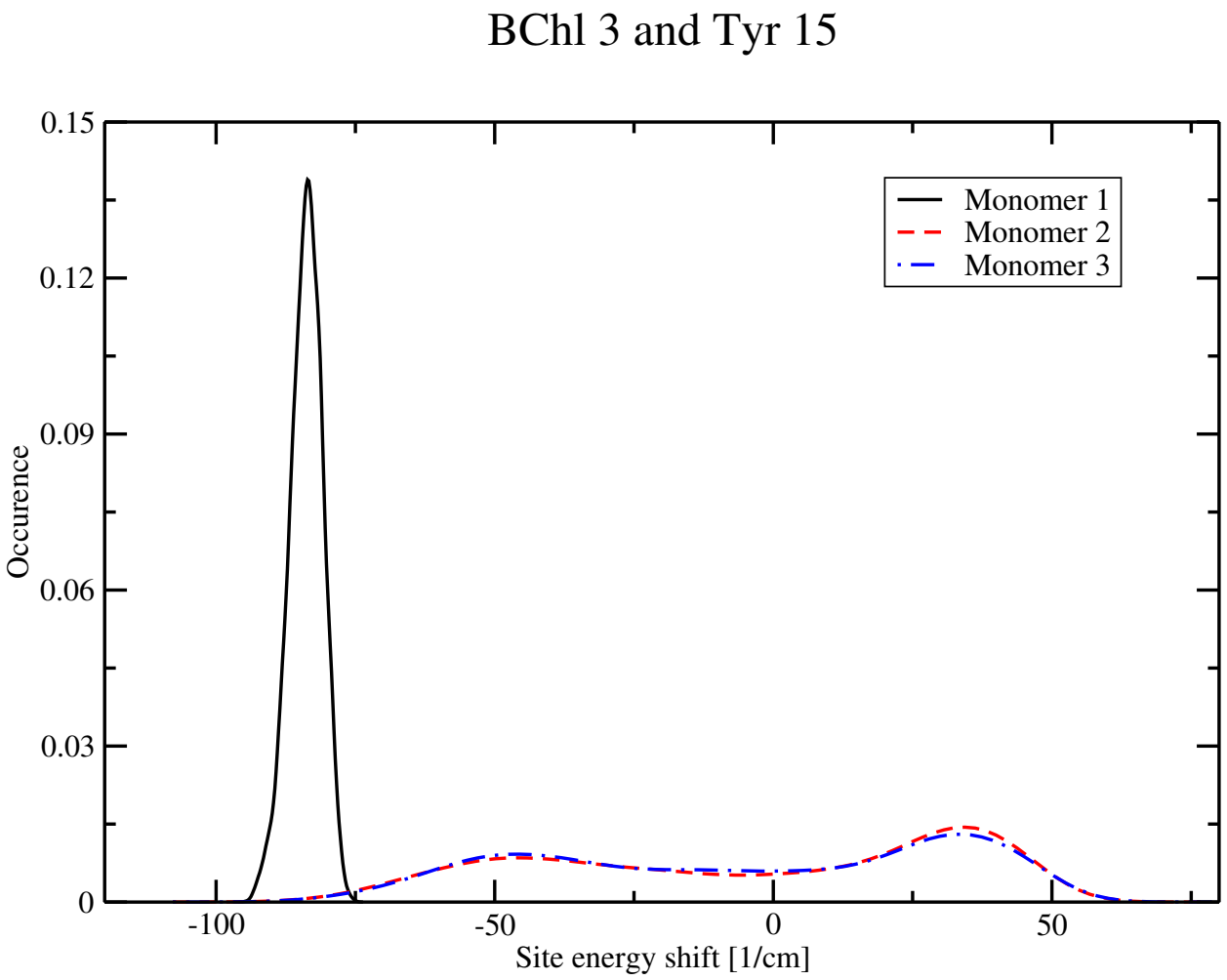

Figure S8: Distribution of site energy shift of BChl 3 caused by Tyr-15 in the three monomeric subunits of the FMO protein, obtained from histograms of $\Delta E_3^{(\mathrm{Tyr15})}$ (Eq. 4 of the main text).

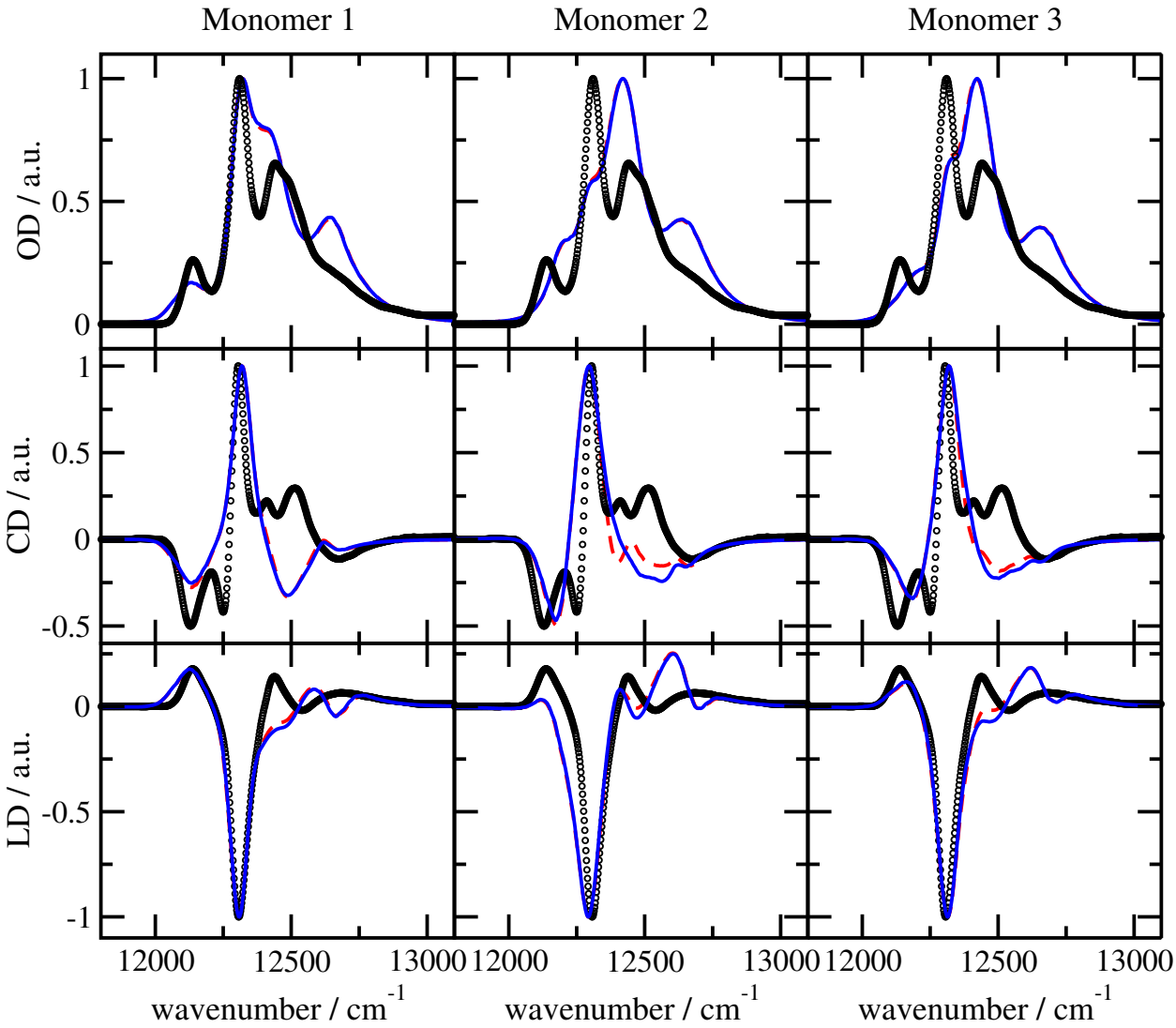

Figure S9: Low temperature (4 K) optical spectra of the three monomeric subunits of the FMO protein, calculated by neglecting (blue solid lines) or taking into account (red-dashed lines) static disorder in excitonic couplings (quantified in Table S4), are compared with experimental data[S12] (black circles).

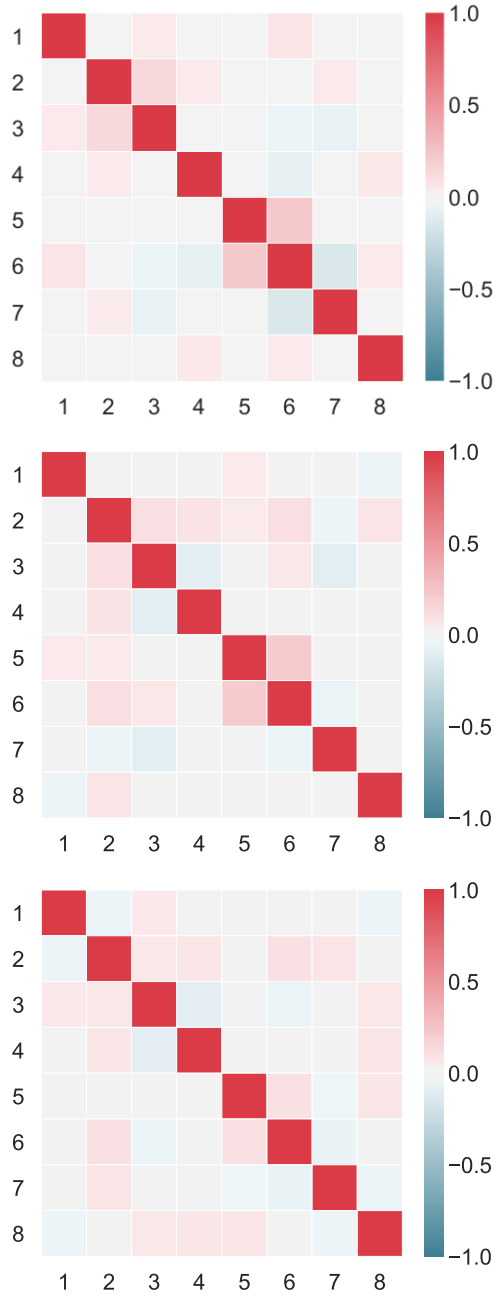

Figure S10: Pearson correlation coefficient for the static disorder in site energies of the 8 BChl pigments of monomer 1 (upper part), monomer 2 (middle part), and monomer 3 (lower part) of the FMO protein.

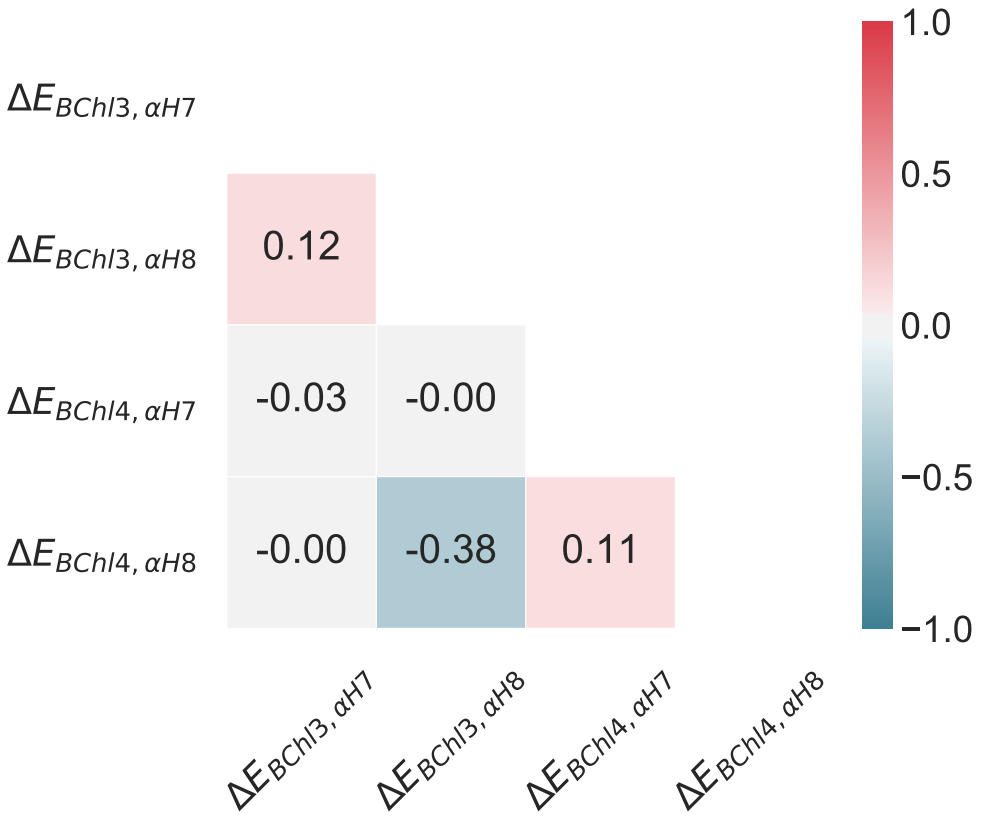

Figure S11: Pearson correlation coefficient for the static disorder in site energies of BChls 3 and 4 caused by the backbone of α-helices H7 and H8 (for the location of these helices in the FMO protein, see Fig. 1 of ref.[S13]).

Table S2: Atomic partial charges $q_I(0,0)$ and $q_I(1,1)$ of the charge density of the electronic ground- and excited state, respectively, of geometry-optimized planar BChl a. The partial charges were obtained in ref.[S5] from a fit of the electrostatic potential (ESP) of the respective charge density obtained with (time-dependent) density functional theory, using the B3LYP exchange correlation functional and a 6-31G* basis set. Please note that the charges reported in the SI of ref.[S5] were obtained by using only the non-hydrogen atom positions in the fit of the ESP. Here, we report the charges obtained including the hydrogen atoms.

I	Atom	$q_I(0,0)$	$q_I(1,1)$	I	Atom	$q_I(0,0)$	$q_I(1,1)$	I	Atom	$q_I(0,0)$	$q_I(1,1)$
1	MG	1.262	1.244	48	C3C	-0.008	0.000	95	C6	-0.180	-0.180
2	CHA	0.367	0.319	49	H3C	0.104	0.105	96	H61	0.090	0.090
3	CHB	-0.457	-0.496	50	C4C	0.429	0.501	97	H62	0.090	0.090
4	HB	0.159	0.161	51	CMC	-0.181	-0.168	98	C7	-0.180	-0.180
5	CHC	-0.720	-0.782	52	1HMC	0.069	0.067	99	H71	0.090	0.090
6	HC	0.311	0.311	53	2HMC	0.069	0.067	100	H72	0.090	0.090
7	CHD	-0.680	-0.715	54	3HMC	0.069	0.067	101	C8	-0.090	-0.090
8	HD	0.223	0.222	55	CAC	-0.315	-0.315	102	H81	0.090	0.090
9	NA	-0.545	-0.587	56	1HAC	0.127	0.128	103	C9	-0.270	-0.270
10	C1A	0.065	0.105	57	2HAC	0.127	0.128	104	H91	0.090	0.090
11	C2A	-0.242	-0.242	58	CBC	-0.164	-0.165	105	H92	0.090	0.090
12	H2A	0.238	0.242	59	1HBC	0.065	0.065	106	H93	0.090	0.090
13	C3A	-0.218	-0.218	60	2HBC	0.065	0.065	107	C10	-0.180	-0.180
14	H3A	0.202	0.204	61	3HBC	0.065	0.065	108	1H10	0.090	0.090
15	C4A	0.479	0.522	62	ND	-0.598	-0.618	109	2H10	0.090	0.090
16	CMA	-0.395	-0.382	63	C1D	0.416	0.484	210	C11	-0.180	-0.180
17	1HMA	0.127	0.125	64	C2D	0.234	0.216	111	1H11	0.090	0.090
18	2HMA	0.127	0.125	65	C3D	-0.412	-0.412	112	2H11	0.090	0.090
19	3HMA	0.127	0.125	66	C4D	-0.032	0.040	113	C12	-0.180	-0.180
20	CAA	-0.315	-0.315	67	CMD	-0.578	-0.570	114	1H12	0.090	0.090
21	1HAA	0.147	0.148	68	1HMD	0.171	0.170	115	2H12	0.090	0.090
22	2HAA	0.147	0.148	69	2HMD	0.171	0.170	116	C13	-0.090	-0.090
23	CBA	-0.198	-0.190	70	3HMD	0.171	0.170	117	1H13	0.090	0.090
24	1HBA	0.052	0.050	71	CAD	0.902	0.871	118	C14	-0.270	-0.270
25	2HBA	0.052	0.050	72	OBD	-0.601	-0.612	119	1H14	0.090	0.090
26	CGA	0.942	0.942	73	CBD	-0.755	-0.747	220	2H14	0.090	0.090
27	O1A	-0.654	-0.656	74	HBD	0.207	0.206	121	3H14	0.090	0.090
28	O2A	-0.416	-0.417	75	CGD	0.903	0.905	122	C15	-0.180	-0.180
29	NB	-0.699	-0.714	76	O1D	-0.625	-0.627	123	1H15	0.090	0.090
30	C1B	0.178	0.208	77	O2D	-0.338	-0.342	124	2H15	0.090	0.090
31	C2B	0.368	0.330	78	CED	-0.313	-0.310	125	C16	-0.180	-0.180
32	C3B	-0.630	-0.663	79	1HED	0.170	0.168	126	1H16	0.090	0.090
33	C4B	0.606	0.681	80	2HED	0.170	0.168	127	2H16	0.090	0.090
34	CMB	-0.647	-0.640	81	3HED	0.170	0.168	128	C17	-0.180	-0.180
35	1HMB	0.182	0.181	82	C1	-0.170	-0.170	129	1H17	0.090	0.090
36	2HMB	0.182	0.181	83	H11	0.177	0.17	230	2H17	0.090	0.090
37	3HMB	0.182	0.181	84	H12	0.177	0.17	131	C18	-0.090	-0.090
38	CAB	0.939	0.915	85	C2	-0.410	-0.410	132	1H18	0.090	0.090
39	OBB	-0.633	-0.647	86	H21	0.139	0.139	133	C19	-0.270	-0.270
40	CBB	-0.732	-0.736	87	C3	0.055	0.055	134	1H19	0.090	0.090
41	1HBB	0.190	0.191	88	C4	-0.244	-0.244	135	2H19	0.090	0.090
42	2HBB	0.190	0.191	89	H41	0.108	0.108	136	3H19	0.090	0.090
43	3HBB	0.190	0.191	90	H42	0.108	0.108	137	C20	-0.270	-0.270
44	NC	-0.629	-0.675	91	H43	0.108	0.108	138	1H20	0.090	0.090
45	C1C	0.524	0.573	92	C5	0.118	0.118	139	2H20	0.090	0.090
46	C2C	-0.218	-0.218	93	H51	0.009	0.009	140	3H20	0.090	0.090
47	H2C	0.132	0.135	94	H52	0.009	0.009				

Table S3: Atomic transition charges $q_I(1,0)$ of the transition density of the $S_0 \rightarrow S_1$ transition of geometry-optimized planar BChl *a*. The partial charges were obtained in ref.[S5] from a fit of the electrostatic potential (ESP) of the transition density obtained with (time-dependent) density functional theory, using the B3LYP exchange correlation functional and a 6-31G* basis set. Please note that the charges reported in the SI of ref.[S5] are unscaled. Here, we report rescaled charges that take into account the experimental value (37.1 D^2)[S6] of the vacuum dipole strength of BChl *a* and a screening and local field correction factor of 0.8.[S3]

I	Atom	$q_I(1,0)$	I	Atom	$q_I(1,0)$
1	MG	0.02669	25	CBB	-0.01204
2	CHA	-0.08946	26	NC	-0.01066
3	CHB	0.00948	27	C1C	-0.05121
4	CHC	0.02872	28	C2C	0.01214
5	CHD	-0.02597	29	C3C	-0.01773
6	NA	-0.04141	30	C4C	0.07369
7	C1A	0.08522	31	CMC	-0.00492
8	C2A	-0.01228	32	CAC	-0.00055
9	C3A	-0.00172	33	CBC	0.00610
10	C4A	-0.01078	34	ND	-0.08538
11	CMA	-0.00737	35	C1D	0.07051
12	CAA	0.01006	36	C2D	0.01416
13	CBA	-0.00598	37	C3D	-0.02332
14	CGA	0.00320	38	C4D	0.12691
15	O1A	-0.00343	39	CMD	0.01985
16	O2A	0.00231	40	CAD	0.02270
17	NB	0.01784	41	OBD	0.01323
18	C1B	-0.05542	42	CBD	0.00148
19	C2B	0.00057	43	CGD	0.00128
20	C3B	-0.04265	44	O1D	0.00562
21	C4B	-0.02130	45	O2D	-0.00448
22	CMB	-0.02070	46	CED	0.00497
23	CAB	0.01586	47	C1	-0.00034
24	OBB	-0.02353			

Table S4: Excitonic couplings between BChl m and n within the three monomeric subunits of the FMO protein. $V_{mn}^{\mathrm{PD}}(\mathrm{cr})$ is the coupling obtained in point-dipole approximation using the crystal structure, where the transiton dipole moment was placed at the center of the line connecting the $\mathrm{N_B}$ and the $\mathrm{N_D}$ atoms of the pigments and the transiton dipole moment was assumed to be directed along this line. The $< V_{mn} >$ and FWHM characterize the center and the full width at half maximum, respectively, of the Gaussian distribution functions obtained for the excitonic couplings with the FRODA-TrEsp method. In this method, the FRODA Monte Carlo sampling of protein conformations was combined with the TrEsp calculations of excitonic couplings. The numbers in brackets for monomer 1 give the corresponding values in point-dipole approximation (taken from Table 1 of ref[S13]). All energies are given in units of cm^{-1}.

	Monomer 1			Monomer 2			Monomer 3		
$m-n$	$V_{mn}^{\mathrm{PD}}(\mathrm{cr})$	$< V_{mn} >$	FWHM	$V_{mn}^{\mathrm{PD}}(\mathrm{cr})$	$< V_{mn} >$	FWHM	$V_{mn}^{\mathrm{PD}}(\mathrm{cr})$	$< V_{mn} >$	FWHM
1-2	-91.2	-105.8 (-92.8)	26.3 (18.4)	-91.6	-99.2	29.2	-91.8	-97.5	31.1
1-3	5.1	6.0 (5.8)	1.7 (1.6)	5.1	4.9	1.8	5.7	5.2	1.8
1-4	-5.9	-6.4 (-5.9)	1.5 (1.4)	-6.0	-6.1	1.4	-6.8	-6.4	1.5
1-5	6.4	8.0 (7.1)	2.3 (2.1)	6.4	7.9	2.2	8.0	7.7	2.3
1-6	-15.3	-22.1 (-14.6)	12.8 (10.6)	-15.4	-24.3	13.0	-15.1	-23.1	13.0
1-7	-11.5	-7.8 (-9.8)	4.9 (4.7)	-11.5	-8.9	5.1	-9.9	-7.9	4.9
1-8'	40.9	23.3	12.0	41.1	25.2	12.6	31.5	23.8	12.5
2-3	30.5	32.8 (29.4)	5.5 (4.7)	30.6	31.5	6.0	31.5	32.8	6.2
2-4	8.0	7.2 (6.4)	2.0 (1.9)	8.1	7.04	1.9	7.0	7.0	2.1
2-5	1.1	1.3 (1.4)	2.9 (2.8)	1.1	1.5	2.7	1.8	1.7	2.9
2-6	13.1	12.2 (10.9)	3.2 (2.8)	13.1	11.2	4.3	7.3	10.5	4.5
2-7	7.3	2.9 (2.7)	6.0 (6.8)	7.3	2.0	5.8	-1.5	0.9	6.2
2-8'	6.4	3.7	2.9	6.4	4.1	3.2	1.2	4.0	3.0
3-4	-56.9	-60.3 (-47.0)	22.2 (30.6)	-57.1	-55.3	26.4	-44.5	-52.1	26.8
3-5	-2.8	1.3 (-0.1)	3.4 (1.5)	-2.8	1.0	.8	-3.3	1.5	3.7
3-6	-9.6	-9.2 (-9.4)	1.0 (0.9)	-9.6	-9.1	1.0	-9.1	-9.2	1.1
3-7	0.1	7.4 (15.8)	20.6 (23.5)	0.1	-4.1	18.9	2.5	-1.5	18.9
3-8'	1.1	0.4	0.7	1.1	0.4	0.7	2.3	0.3	0.6
4-5	-70.5	-66.7 (-58.8)	22.6 (17.2)	-70.8	-54.2	19.8	-70.0	-55.9	20.3
4-6	-16.8	-17.7 (-16.1)	4.2 (3.5)	-16.9	-17.2	3.7	-15.4	-17.1	3.9
4-7	-62.1	-65.8 (-63.1)	24.0 (17.4)	-62.4	-63.1	22.6	-67.1	-67.8	22.2
4-8'	-1.7	-1.6	0.7	-1.7	-1.6	0.6	-1.3	-1.6	0.6
5-6	80.1	79.9 (91.3)	33.4 (33.0)	80.5	85.1	28.9	87.8	87.0	28.3
5-7	-2.2	5.5 (-2.6)	12.9 (12.7)	-2.2	2.4	12.1	-5.8	2.7	12.3
5-8'	4.2	3.8	0.8	4.2	4.1	0.8	5.8	4.1	0.7
6-7	39.4	35.5 (35.0)	13.2 (13.4)	39.6	34.3	14.0	41.1	34.3	14.1
6-8'	-8.9	-9.0	4.0	-9.0	-9.9	3.7	-7.0	-10.5	3.6
7-8'	-10.8	-7.9	2.2	-10.9	-11.3	1.9	-8.1	-11.3	1.8

References

(S1) Renger, T.; Klinger, A.; Steinecker, F.; Schmidt am Busch, M.; Numata, J.; Müh, F. Normal Mode Analysis of the Spectral Density of the Fenna-Matthews-Olson Light-Harvesting Protein: How the Protein Dissipates the Excess Energy of Excitons. *J. Phys. Chem. B* **2012**, *116*, 14565–14580.

(S2) Renger, T.; Marcus, R. A. On the relation of protein dynamics and exciton relaxation in pigment-protein complexes: an estimation of the spectral density and a theory for the calculation of optical spectra. *J. Chem. Phys.* **2002**, *116*, 9997–10019.

(S3) Adolphs, J.; Renger, T. How proteins trigger excitation energy transfer in the FMO complex of green sulfur bacteria. *Biophys. J.* **2006**, *91*, 2778–2797.

(S4) Renger, T.; May, V. Simulations of frequency-domain spectra: Structure-function relationships in photosynthetic pigment-protein complexes. *Phys. Rev. Lett.* **2000**, *84*, 5228–5231.

(S5) Madjet, M. E.; Abdurahman, A.; Renger, T. Intermolecular Coulomb couplings from ab initio electrostatic potentials: application to optical transitions of strongly coupled pigments in photosynthetic antennae and reaction centers. *J. Phys. Chem. B* **2006**, *110*, 17268–17281.

(S6) Knox, R. S.; Spring, B. Q. Dipole strengths in the chlorophylls. *Photochem. Photobiol.* **2003**, *77*, 497–501.

(S7) Tronrud, D. E.; Wen, J.; Gay, L.; Blankenship, R. E. The structural basis for the difference in absorbance spectra for the FMO antenna protein from various green sulfur bacteria . *Photosynth. Res.* **2009**, *100*, 79–87.

(S8) Schmidt am Busch, M.; Müh, F.; Madjet, M. E.; Renger, T. The Eighth Bacteri-

ochlorophyll Completes the Excitation Energy Funnel in the FMO Protein. *J. Phys. Chem. Lett.* **2011**, *2*, 93–98.

(S9) Saito, S.; Higashi, M.; Fleming, G. R. Site-Dependent Fluctuations Optimize Electronic Energy Transfer in the Fenna-Matthews-Olson Protein. *J. Phys. Chem. B* **2019**, *123*, 9762–9772.

(S10) Jurinovich, S.; Curutchet, C.; Mennucci, B. The Fenna-Matthews-Olson Protein Revisited: A Fully Polarizable (TD)DFT/MM Description. *Chem. Phys. Chem.* **2014**, *15*, 3194–3204.

(S11) Kim, Y.; Morozov, D.; Stadnytski, S., V. Savikhin; Slipchenko, L. V. Predictive First-Principles Modeling of a Photosynthetic Antenna Protein: The Fenna-Matthews-Olson Complex. *J. Phys. Chem. Lett.* **2020**, *11*, 1636–1643.

(S12) Wendling, M.; Przyjalgowski, M. A.; Gülen, D.; Vulto, S. I. E.; Aartsma, T. J.; van Grondelle, R.; van Amerongen, H. The quantitative relationship between structure and polarized spectroscopy in the FMO complex of *Prosthecochloris aestuarii*: refining experiments and simulations. *Photosynth. Res.* **2002**, *71*, 99–123.

(S13) Fokas, A. S.; Cole, D. J.; Chin, A. W. Constrained geometric dynamics of the Fenna-Matthews-Olson complex: the role of correlated motion in reducing uncertainty in excitation energy transfer. *Photosynth. Res.* **2014**, *122*, 275–292.